Femtosecond laser-inscribed waveguides in Nd^{3+}:Y^{3+}:SrF_2 crystals

Shengzhi Sun (孙盛芝)[1], Liangbi Su (苏良碧)[2], Yufeng Yuan (袁玉峰)[1], and Zhenrong Sun (孙真荣)[1*]

[1]*State Key Laboratory of Precision Spectroscopy, and Department of Physics, East China Normal University, Shanghai 200062, China*

[2]*Key Laboratory of Transparent and Opto-Functional Advanced Inorganic Materials, Shanghai Institute of Ceramics, Chinese Academy of Sciences, Shanghai 201800, China*

[*]*Corresponding author: zrsun@phy.ecnu.edu.cn*

Received August 14, 2013; accepted September 16, 2013; posted online November 4, 2013

Optical waveguides are fabricated in Nd^{3+}:Y^{3+}:SrF_2 crystals by a 1-kHz femtosecond laser using the double-line approach. Waveguides with different separations (10, 15, and 20 μm) between two consecutive optical breakdown tracks are produced, and their optical performances are explored by end-fire coupling to 780-and 532-nm lasers. Propagation loss of the waveguide with 20-μm separation is estimated. The micro-photoluminescence and micro-Raman spectra indicate that the original fluorescence and lattice structure of the Nd^{3+}:Y^{3+}:SrF_2 crystals are well preserved in the waveguide. Therefore, the obtained waveguide structures are promising candidate for application in integrated waveguide lasers.

OCIS codes: 230.7380, 140.7090, 160.3380.
doi: 10.3788/COL201311.112301.

As a basic component of integrated photonics, optical waveguides provide a foundation for building-up relatively low lasing thresholds and high-efficiency waveguide laser systems[1−4]. These waveguides also present the possibility of integrating various devices on a single chip to achieve multifunctional photonic applications[5−7]. Several techniques for waveguide fabrication, such as ion exchange[8], ion implantation[9], diffusion of metal ions[10], laser inscription[11,12], and femtosecond laser-inscription[11−13], have been developed. Among these techniques, femtosecond laser inscription has emerged as a highly efficient method for waveguide fabrication in transparent materials, such as optical crystals[14,15], ceramics[16,17] and glasses[18,19]. It is also attractive for its strong three-dimensional (3D) ability to achieve more complicated structures.

Femtosecond laser-inscribed optical waveguides usually have four structures: directly written waveguides (type I)[20,21], stress-induced waveguides (type II)[21−23], depressed cladding waveguides (type III)[16,24], and ablated ridge waveguides (type IV)[25]. Stress-induced waveguides (type II) are one of the most mature and commonly used waveguide structures. Most of these waveguides are constructed via a "double-line" approach. During laser fabrication, micro-explosions take place at the focal point of the laser pulse, leading to volume expansion in the optical breakdown tracks and residual stress in the surrounding regions. Thus, a permanent change in refraction index is induced in the guiding region between the two parallel tracks. By total internal reflection, light can be confined and propagated in the guiding region.

Because of the long radiative lifetime of Nd^{3+} in the $^4F_{3/2}$ state, relatively low pump thresholds, and fewer constraining temperature effects, Nd^{3+} doped oxides and fluoride crystals are considered promising laser host media for producing wavelengths of around 1 μm. Besides the widely used Nd^{3+}:YAG, Nd^{3+} doped fluoride crystals (Nd^{3+}:CaF_2, Nd^{3+}:SrF_2, and Nd^{3+}:BaF_2) have attracted significant attention for their considerable advantages, which include long emission time, broad absorption/emission spectrum, and capacity to grow to large sizes with high optical quality[26,27]. Nd^{3+}:SrF_2 crystals are very interesting materials for diode pumped solid-state lasers and laser amplifiers[27,28]. Unlike in Nd^{3+}:CaF_2[27], the concentration quenching effect in Nd^{3+}:SrF_2 is much weaker because the crystals show low levels of aggregation and the pair rhombic site ($NdF)_2$ features large ion to ion distances[29]. Nd^{3+}:Y^{3+} codoped SrF_2 has been considered a potential laser material since it is reported that codoping Y^{3+} "buffer" ions in Nd^{3+} doped fluoride crystals can dramatically increase photoluminescence efficiency by depressing aggregation, thereby broadening the absorption band and lengthening the emission lifetime[27,30].

In this letter, we report the fabrication of channel waveguides in Nd^{3+}:Y^{3+}:SrF_2 crystals using femtosecond laser inscription under a double-line approach. The optical performances of waveguides with different separations (10, 15, and 20 μm) are demonstrated, and the propagation loss (α) of the waveguide with 20-μm separation is estimated. The micro-fluorescence and micro-Raman spectra of the waveguides are also investigated.

The Nd^{3+}:Y^{3+}:SrF_2 (doped with 5% Nd^{3+} and 10% Y^{3+}) crystal used in this work was cut to dimensions of 10×10×2 (mm), and its four faces were polished up to optical quality. The channel waveguides were fabricated with a double-line configuration using an amplified Ti: sapphire laser system generating linearly polarized laser pulses centered at 800 nm with an 80-fs pulse width and a 1-kHz repetition rate. The laser beam, propagating along the c axis of the Nd^{3+}:Y^{3+}:SrF_2 crystal, was focused into the sample approximately 150 μm below the surface with a 50× microscope objective (NA=0.8). The sample was fixed on a 3D

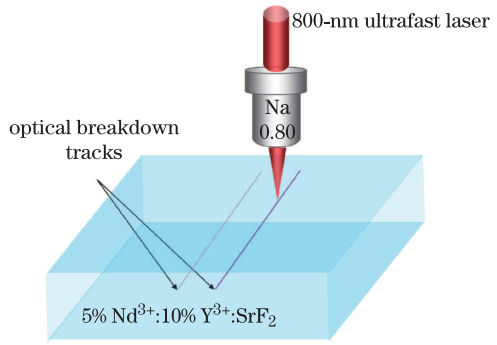

Fig. 1. Schematic diagram of the waveguide fabrication experiment setup.

motorized stage with a spatial resolution of 0.2 μm and translated perpendicular to the laser beam with a speed of 100 μm/s to inscribe tracks under a pulse energy of 1 μJ. Under these conditions, three groups of double tracks with separations of 10, 15, and 20 μm were written. Waveguides were formed in the region between the double tracks by stress-induced refractive index (n) changes. A schematic diagram of the experimental setup for waveguide fabrication is shown in Fig. 1.

An end-face coupling system was utilized to investigate the optical properties of the waveguides. Laser beams with wavelengths of 780 and 532 nm were coupled to the channel waveguides by a 10× microscope objective (N.A.=0.90) to excite the guide modes. Light from the output facet of the sample was collected using a 10× microscope objective (N.A.=0.90), and the output facet was imaged onto a CCD camera. The α of the waveguide was also measured by a similar end-fire coupling system with a 632.8-nm He-Ne laser. Micro-photoluminescence and micro-Raman spectra were obtained using a Raman spectrometer (Jobin Yvon T64000) equipped with a confocal microscope (IX81, Olympus), a 532-nm CW solid state laser, and a 100× microscope objective (NA=0.95).

Microscopic images of the top view of the waveguide structures with 10-, 15-, and 20-μm separations obtained in this experiment are presented in Fig. 2(a). The waveguide region is located between the double tracks and pointed out by the arrow in the images. To obtain smooth laser-induced tracks and achieve good optical performance from the guiding structures, fabrication parameters were optimized. Fig. 2(b) shows microscopic images of the end faces of the waveguides. The dark lines correspond to the laser-induced damage tracks, and the regions between the tracks schematically marked by the dashed circles indicate the guiding regions.

To test the optical performances of the waveguides shown in Fig. 2, two laser beams with different wavelengths (780 and 532 nm) were focused on the waveguides using a homebuilt end-face coupling system. Field distributions of the guided TM modes in waveguides with different separations are presented in Fig. 3. The 780- and 532-nm lasers were both guided between the double tracks. The waveguide with 10-μm separation shows no confinement for the 780-nm laser beam, which may indicate that the coupling efficiency of the waveguides in this experiment is better for lasers with shorter-wavelength than for those with longer-wavelength. As the intensity of the input laser beam is equal

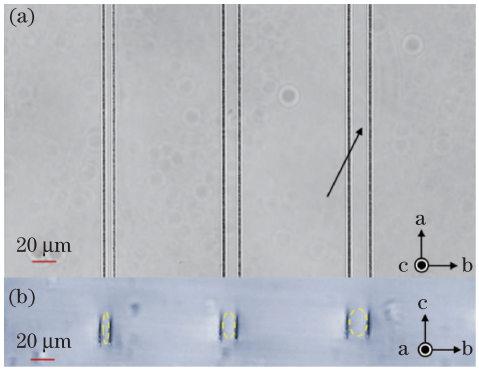

Fig. 2. Optical micrographs of the (a) top views and (b) end faces of the waveguides fabricated with double-line separations of 10, 15, and 20 μm.

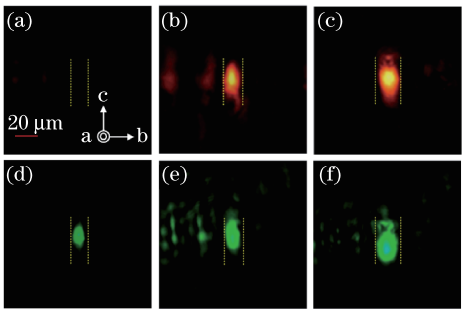

Fig. 3. Output TM laser mode profiles of the (a, d) 10-, (b, e) 15-, and (c, f) 20-μm waveguides coupled to (a)–(c) 780- and (d)–(f) 532-nm lasers. The location of the damage tracks is systematically indicated by yellow dashed lines.

for all of the waveguides, the α obviously decreases as the track separation increases from 10 to 20 μm.

The α of the waveguides were measured by end-fire coupling 632.8-nm laser beams with equal laser power to waveguides of different lengths[31] and measuring the transmitted power of every single waveguide. In this experiment, we began measurement with a relatively long waveguide sample. The sample was then shortened by cutting and polishing into three different lengths. The α was calculated from the following equation:

$$\alpha = \frac{\ln(P_1 - P_2)}{Z_2 - Z_1}, \text{ for } Z_2 > Z_1, \tag{1}$$

where P_1 and P_2 are the transmitted powers of waveguides with two different lengths Z_1 and Z_2, respectively. The average value was obtained as the final α. Using this method, the α of the waveguide with a separation of 20 μm may be estimated to be ~3.2 dB/cm in TM mode and ~3.8 dB/cm in TE mode at 632.8 nm.

Compared with type II waveguides fabricated in other optical crystals, such as BGO (~4.2 dB/cm)[32], Yb:KYW (~3.9 dB/cm)[33], BiB_3O_6(~5 dB/cm)[34] and $YLiF_4$(~4 dB/cm)[35], the α of our waveguide in the Nd^{3+}:Y^{3+}:SrF_2 system is acceptable. Since waveguide lasers are built with several waveguides fabricated in Nd^{3+} doped crystals with relatively high α, for instance, Nd:YAG (~3.8 dB/cm)[36], Nd:GGG (~4.5 dB/cm)[25], and Nd:LGS (~5.6 dB/cm)[24], the waveguide in the Nd^{3+}:Y^{3+}:SrF_2 system can be considered a promising candidate for developing waveguide lasers.

The change in n (Δn) in the waveguide can be roughly estimated using the formula[11]:

$$\Delta n = \sin^2 \Theta_{\mathrm{m}}/2n, \quad (2)$$

where n is the refractive index of the unstructured sample and Θ_{m} is the maximum beam divergence of entering or leaving the waveguide. In our system, the n of the sample is about 1.43, which is approximately equal to that of the Nd^{3+}:SrF_2 system[27]. The Θ_{m} of the waveguide with 20-μm separation is around 2° with an error of 30%. Thus, the Δn in the core region of 20-μm waveguide is in the order of $\Delta n \approx 8 \times 10^{-4}$.

As a potential candidate for solid-state lasers, the spectroscopic properties of the Nd^{3+}:Y^{3+}:SrF_2 waveguide were analyzed in detail. Figure 4 shows the micro-photoluminescence spectra of the guiding region, the damage track, and the unmodified (bulk) region in the Nd^{3+}:Y^{3+}:SrF_2 system with two emission bands at 840–900 and 1 010–1 075 nm, which correspond to the $^4F_{3/2} \rightarrow {}^4F_{9/2}$ and $^4F_{3/2} \rightarrow {}^4I_{11/2}$transitions, respectively. In general, Nd^{3+} ions in the Nd^{3+}:Y^{3+}:SrF_2 system show good photoluminescence efficiencies even with a high doping concentration of 5%. This finding indicates that Y^{3+} buffer ions reduce the concentration quenching effect in Nd^{3+} doped fluoride crystals efficiently[30]. Moreover, the emission band at 1 010–1 075 nm has three obvious peaks at 1 037, 1 046, and 1 052 nm, respectively.

Two luminescence centers, known as the L and M centers, are identified in the Nd^{3+} doped SrF_2 system[27]. The tetragonal L-centers have emission peaks at 1 037, 1 046, and 1 052 nm with long emission lifetimes, whereas the clustered M-centers have emission peaks at 1 046 and 1 060 nm with shorter emission lifetimes[37]. The signals in Fig. 4 indicate that tetragonal L-center fluorescence dominates the Nd^{3+}:Y^{3+}:SrF_2 system, which is quite interesting for a heavily doped Nd^{3+} fluoride system. This phenomenon can be attributed to the codoping of Y^{3+} buffer ions, which can transform weakly luminescent [Nd^{3+}-Nd^{3+}] clusters into more intense [Nd^{3+}-Y^{3+}] active centers[30]. In addition, the emission spectrum of the Nd^{3+}:Y^{3+}:SrF_2 system contains four narrow peaks located at 859, 865, 1 046, and 1 052 nm, respectively, thereby presenting the possibility of lasing at different wavelengths.

The micro-photoluminescence spectra of the guiding and bulk regions of the Nd^{3+}:Y^{3+}:SrF_2 system are substantially similar, which indicates that the original fluorescence property of the Nd^{3+}:Y^{3+}:SrF_2 system is well preserved in the waveguide, a property that is very important for a candidate of waveguide laser. The drop in photoluminescence intensity in the damage track may result from defects in the Nd^{3+}:Y^{3+}:SrF_2 crystal caused by the inscription process[22]. During laser fabrication, the material at the focal point melts under high temperature; as soon as this material cools, it recrystallizes and induces a large number of defects in the lattice structure, which leads to poor photoluminescence efficiency[11].

The micro-Raman spectra of the guiding region, damage track, and bulk region were obtained to analyze the lattice vibration mode of the Nd^{3+}:Y^{3+}:SrF_2 system. Figure 5 shows that only the spectrum intensity of the damage track presents a significant

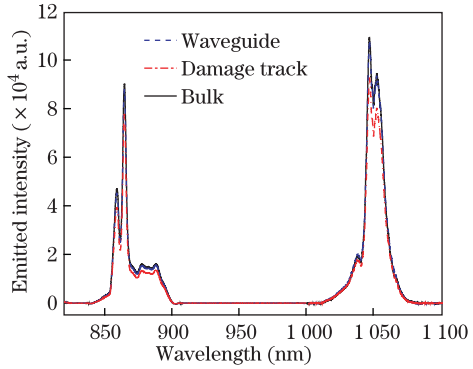

Fig. 4. Micro-photoluminescence spectra corresponding to $^4F_{3/2} \rightarrow {}^4F_{9/2}$ and $^4F_{3/2} \rightarrow {}^4I_{11/2}$ transitions obtained from the unmodified Nd^{3+}:Y^{3+}:SrF_2 area (bulk), the damage track, and the guiding region at room temperature.

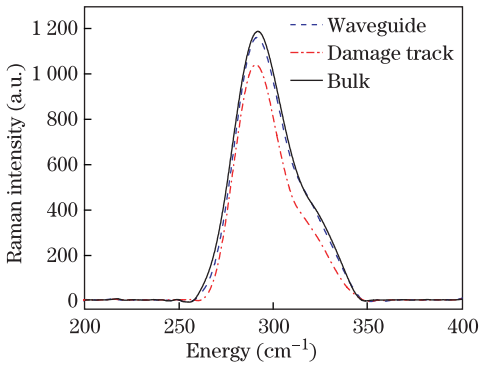

Fig. 5. Micro-Raman spectra obtained from the unmodified Nd^{3+}:Y^{3+}:SrF_2 area (bulk), the damage track, and the guiding region.

drop, which may be attributed to defects in the Nd^{3+}:Y^{3+}:SrF_2 crystal, as described in our micro-photoluminescence spectrum analysis. This finding indicates that the guiding region substantially retains the lattice structure and Raman efficiency of the bulk region of the Nd^{3+}:Y^{3+}:SrF_2 system.

Interestingly, Raman modes in the damaged track and guiding area show a slight blue shift when compared with that of the bulk region. This blue shift proves the existence of stress generated by the laser inscription process in the damaged tracks and surrounding areas. The Raman mode may shift to higher vibration energies upon application of compressive stress[22]. Therefore, the blue shift of Raman modes in the damage track and guiding region could be attributed to local compression stresses of the Nd^{3+}:Y^{3+}:SrF_2 network. For the local stress to decreases as the distance from the damage track increases, the vibration energy of the Raman mode in the guiding region must be lower than that in the damage track. In fact, the blue shift in the guiding region (about 0.3 cm^{-1}) is fairly minimal that the residual stress may be considered to have little impact on the lattice structure in the guiding region. A similar phenomenon has been observed in waveguides written in the Nd^{3+}:YVO_4 system[22].

In conclusion, buried waveguides have been fabricated in Nd^{3+}:Y^{3+}:SrF_2 crystals by the double-line approach using the femtosecond laser inscription method. The obtained waveguides show good light confinement and

relatively low α at a separation of 20 μm (~3.2 dB/cm in TM mode and ~3.8 dB/cm in TE mode at 632.8 nm). The micro-photoluminescence and micro-Raman spectra of the guiding and bulk regions have been explored, and similar spectra indicate that both the fluorescence properties and lattice structure of the Nd^{3+}:Y^{3+}:SrF_2 system are well preserved in the guiding region. Thus, femtosecond laser-written waveguides in Nd^{3+}:Y^{3+}:SrF_2 are potential candidate for the development of integrated waveguide lasers.

This work was supported by the National Natural Science Foundation of China (Nos. 11004060, 11027403, 51132004, 61178056, and 91222112).

References

1. C. Grivas, Prog. Quantum Electron. **35,** 159 (2011).
2. L. Miao, D. Zuo, Z. Jiu, Z. Cheng, C. Qi, and J. Wu, Chin. Opt. Lett. **8,** 411 (2010).
3. W. Guo, J. Liu, J. Chen, L. Li, L. Wang, F. Liu, and Z. Wang, Chin. Opt. Lett. **9,** 061404 (2011).
4. J. Zhang, L. Liu, W. Chen, A. Liu, W. Zhou, and W. Zheng, Chin. Opt. Lett. **10,** 061401 (2012).
5. Q. Zhao, K. Cui, X. Feng, Y. Huang, Y. Li, D. Zhang, and W. Zhang, Chin. Opt. Lett. **11,** 031301 (2013).
6. F. Chen, Laser Photon. Rev. **6,** 622 (2012).
7. X. Ma, J. He, and M. Li, Chin. Opt. Lett. **11,** 032501 (2013).
8. L. P. Shi, T. C. Chong, Z. Zhuo, W. X. Hou, and P. F. Hu, Appl. Phys. Lett. **71,** 2737 (1997).
9. F. Chen, J. Appl. Phys. **106,** 081101 (2009).
10. Y. L. Lee, T. J. Eom, W. Shin, B. Yu, D. Ko, W. Kim, and H. Lee, Opt. Express **17,** 10718 (2009).
11. J. Siebenmorgen, K. Petermann, G. Huber, K. Rademaker, S. Nolte, and A. Tünnermann, Appl. Phys. B **97,** 251 (2009).
12. R. R. Thomson, S. Campbell, I. J. Blewett, A. K. Kar, and D. T. Reid, Appl. Phys. Lett. **88,** 111109 (2006).
13. F. Chen and J. R. Vázquez de Aldana, Laser Photon. Rev. **1-26** (2013).
14. Y. Tan, F. Chen, J. R. Vázquez de Aldana, G. A. Torchia, A. Benayas, and D. Jaque, Appl. Phys. Lett. **97,** 031119 (2010).
15. A. Rodenas and A. K. Kar, Opt. Express **19,** 17820 (2011).
16. H. Liu, Y. Jia, J. Rodríguez Vázquez de Aldana, D. Jaque, and F. Chen, Opt. Express **20,** 18620 (2012).
17. G. A. Torchia, A. Rodenas, A. Benayas, E. Cantelar, L. Roso, and D. Jaque, Appl. Phys. Lett. **92,** 111103 (2008).
18. N. D. Psaila, R. R. Thomson, H. T. Bookey, A. K. Kar, N. Chiodo, R. Osellame, G. Cerullo, A. Jha, and S. Shen, Appl. Phys. Lett. **90,** 131102 (2007).
19. D. G. Lancaster, S. Gross, H. Ebendorff-Heidepriem, K. Kuan, T. M. Monro, M. Ams, A. Fuerbach, and M. J. Withford, Opt. Lett. **36,** 1587 (2011).
20. M. Ams, G. D. Marshall, and M. J. Withford, Opt. Express **14,** 13158 (2006).
21. J. Burghoff, S. Nolte, and A. Tünnermann, Appl. Phys. A. **89,** 127 (2007).
22. W. F. Silva, C. Jacinto, A. Benayas, J. R. Vazquez de Aldana, G. A. Torchia, F. Chen, Y. Tan, and D. Jaque, Opt. Lett. **35,** 916 (2010).
23. S. M. Eaton, C. A. Merchant, R. Iyer, A. J. Zilkie, A. S. Helmy, J. S. Aitchison, P. R. Herman, D. Kraemer, R. J. D. Miller, C. Hnatovsky, and R. S. Taylor, Appl. Phys. Lett. **92,** 081105 (2008).
24. Y. Ren, J. R. Vázquez de Aldana, F. Chen, and H. Zhang, Opt. Express **21,** 6503 (2013).
25. Y. Jia, N. Dong, F. Chen, J. R. V'azquez de Aldana, Sh. Akhmadaliev, and S. Zhou, Opt. Express **20,** 9763 (2012).
26. C. R. A. Catlow, A. V. Chadwick, G. N. Greaves, and L. M. Moroney, Nature **312,** 601 (1984).
27. S. A. Payne, J. A. Caird, L. L. Chase, L. K. Smith, N. D. Nielsen, and W. F. Krupke, J. Opt. Soc. Am. B **8,** 726 (1991).
28. A. A. Kaminskii, *Laser Crystals* (Springer-Verlag, New York, 1981).
29. V. V. Osiko, Yu. K. Voron'ko, and A. A. Sobol, Crystals **10,** 37 (1984).
30. L. B. Su, Q. G. Wang, H. J. Li, G. Brasse, P. Camy, J. L. Doualan, A. Braud, R. Moncorgé, Y. Y. Zhan, L. H. Zheng, X. B. Qian, and J. Xu, Laser Phys. Lett. **10,** 035804 (2013).
31. R. G. Hunsperger, *Integrated Optics: Theory and Technology* (Springer, Newark, USA, 2009).
32. B. Qian, Y. Liao, G. Dong, F. Luo, L. Su, S. Sun, and J. Qiu, Chin. Phys. Lett. **26,** 070601 (2009).
33. F. M. Bain, W. F. Silva, A. A. Lagatsky, R. R. Thomson, and N. D. Psaila, Appl. Phys. Lett. **98,** 141108 (2011).
34. S. J. Beecher, R. R. Thomson, D. T. Reid, N. D. Psaila, M. Ebrahim-Zadeh, and A. K. Kar, Opt. Lett. **36,** 4548 (2011).
35. X. Liu, S. Qu, Y. Tan, and F. Chen, J. Phys. D: Appl. Phys. **44,** 495101 (2011).
36. Y. Jia, N. Dong, F. Chen, J. R. Vázquez de Aldana, S. Akhmadaliev, and S. Zhou, Opt. Mater. Express **2,** 657 (2012).
37. O. K. Alimov, T. T. Basiev, M. E. Doroshenko, P. P. Fedorov, V. A. Konyushkin, A. N. Nakladov, and V. V. Osiko, Opt. Mater. **34,** 799 (2012).